Plasma ionization by annularly bounded helicon waves

Masayuki Yano[a] and Mitchell L. R. Walker[b]
Department of Aerospace Engineering, Georgia Institute of Technology, Atlanta, Georgia 30332

The general solution to the electrostatic and magnetic fields is derived with respect to the boundary conditions of a coaxial helicon plasma source. The electric field contours suggest that a simple antenna design can ionize the gas in a coaxial configuration. In addition, the power deposition as a function of excitation frequency is derived. The solution is validated by comparison with the standard cylindrical helicon plasma source. Further, a parametric study of source length, channel radius, channel width, and antenna excitation frequency are presented. This study suggests that it is possible to create a helicon plasma source with a coaxial configuration. © *2006 American Institute of Physics.* [DOI: 10.1063/1.2207125]

I. INTRODUCTION

Helicon plasma sources are high efficiency, high density devices that creates a steady-state plasma from a gaseous propellant.[1] Plasma production is sustained by absorption and propagation of helicon waves, or bounded whistler waves, in magnetized plasma through the Landau damping mechanism. To launch the wave into the plasma, an axial magnetic field is applied in the ionization region and an rf antenna surrounding the plasma column couples to the plasma. The magnetic field direction and the antenna geometry determine the resultant wave propagation direction and wave pattern. The absence of electrodes in plasma prevents device failure due to the electrode erosion.

Recent United States Air Force mission designs require electric propulsion devices to operate at high thrust-to-power ratios that may be unachievable with standard Hall effect thruster (HET) configurations.[2] However, modified HETs may perform at this level and maintain their efficiency if a separate plasma source supplies high-density plasma into the acceleration region. Cylindrical helicons possess the plasma density required for a high thrust-to-power HET, but their geometry is not readily incorporated into the annular HET discharge chamber. A solution to this problem is to develop an annular helicon plasma source that feeds directly into the rear of the HET discharge chamber. Thus, this article aims to investigate the feasibility of an annular helicon plasma source through rigorous theoretical analysis. The article provides the solution to the electric and magnetic field with the boundary conditions of a coaxial configuration.

II. DISPERSION RELATION

The derivation of the classical helicon wave dispersion relationship has been reviewed by Chen.[3] Part of that derivation is repeated here for clarity. In the derivation that follows, the displacement current is neglected, and the plasma current is assumed to be carried entirely by the drifting of

electron gyration center. The second assumption is valid if (a) the frequency of helicon waves is much less than the electron cyclotron frequency that electron gyration is too fast to matter, (b) the wave frequency is much higher than the lower hybrid frequency so that ion motions do not contribute, and (c) resistivity is zero. Thus, classical helicon waves exist in the frequency range defined by

$$\omega_{LH} \ll \omega \ll \omega_{ec}. \tag{1}$$

Under the assumptions stated previously, the linearized equations governing the behavior of classical helicon waves are

$$\nabla \times \mathbf{E} = -\frac{\partial \mathbf{B}}{\partial t}, \tag{2}$$

$$\nabla \times \mathbf{B} = \mu_0 \mathbf{j}, \tag{3}$$

$$\mathbf{E} = (\mathbf{j} \times \mathbf{B}_0)/(en_0) \tag{4}$$

where n_0 and $\mathbf{B}_0 = B_0 \hat{z}$ are equilibrium plasma density and magnetic field, and $\mathbf{B}$, $\mathbf{E}$, and $\mathbf{j}$ are the perturbed magnetic field, electric field, and current density, respectively. These equations can be rearranged into

$$\nabla \cdot \mathbf{B} = 0, \tag{5}$$

$$\nabla \cdot \mathbf{j} = 0, \tag{6}$$

$$\mathbf{j}_\perp = -en_0(\mathbf{E} \times \mathbf{B})/B_0^2. \tag{7}$$

If the perturbations are harmonic functions with respect to time and space, they can be expressed in the form of

$$\mathbf{B} = \mathbf{B}(r)e^{i(m\theta + kz - \omega t)}, \tag{8}$$

where m is the mode number, k is the parallel wave number, and ω is the angular frequency of the wave. Figure 1 shows the rotation of the electric field pattern as the wave propagates along the applied magnetic field direction. The mode number determines the direction of the wave pattern rotation seen by a stationary observer; $m > 0$ represents clockwise rotation and $m < 0$ represents counterclockwise rotation. When an antenna is coupled to helicon waves, the antenna length determines the parallel wave number, k, which is in-

[a]Electronic mail: gtg809r@mail.gatech.edu
[b]Mailing address: Assistant Professor, Department of Aerospace Engineering, High-Power Electric Propulsion Laboratory, 449 Guggenheim Building, 270 Ferst Drive, Atlanta, GA 30332.
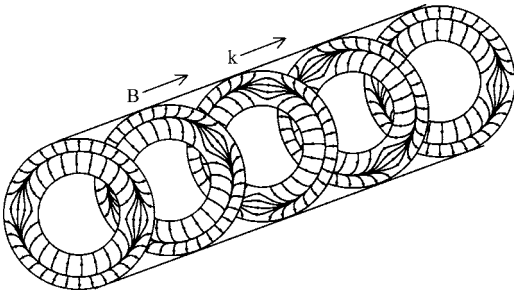
    13, 063501-1

FIG. 1. Electric field pattern rotates both spatially and with time in the $m=1$ mode. The wave propagates in the direction of the applied magnetic field.

versely proportional to the wavelength. Similarly, the antenna driving frequency determines the angular frequency of the wave. Thus, ω/k is the phase velocity of the wave.

Under harmonic perturbation defined by (8), (2) and (4) give

$$i\omega\mathbf{B} = \nabla \times \mathbf{E} = \nabla \times (\mathbf{j} \times \mathbf{B}_0)/(en_0) = (\mathbf{B} \cdot \nabla)\mathbf{j}/(en_0)$$

$$= \mathbf{j}[(ikB_0)/(en_0)]. \tag{9}$$

Then, (3) and (9) yield

$$\nabla \times \mathbf{B} = \mathbf{B}[(\omega/k)(\mu_0 en_0/B_0)]. \tag{10}$$

To simplify the expression, let the quantity in the square brackets equal α, the total wave number. The total wave number can be expressed in terms of electron frequencies

$$\alpha = (\omega/k)(\mu_0 en_0/B_0) = (\omega/k)[\omega_p^2/(\omega_c c^2)]. \tag{11}$$

The equation shows a linear dependence of the plasma density on the applied magnetic field strength for a given phase velocity. Substituting α into (10) yields

$$\nabla \times \mathbf{B} = \alpha\mathbf{B}. \tag{12}$$

The curl of (12) generates the equation that governs the behavior of helicon waves,

$$\nabla^2\mathbf{B} + \alpha^2\mathbf{B} = 0. \tag{13}$$

On the other hand, substituting (12) into (3) yields

$$\mathbf{j} = (\alpha/\mu_0)\mathbf{B}. \tag{14}$$

Thus, the current is parallel to the perturbed magnetic field.

Equation (13) is the Helmholtz differential equation. The radial component of the equation is

$$\frac{\partial^2 B_r}{\partial r^2} + \frac{1}{r}\frac{\partial B_r}{\partial r} + \left(\alpha^2 - k^2 - \frac{m^2-1}{r^2}\right)B_r - \frac{2im}{r^2}B_\theta = 0, \tag{15}$$

where $B_r = B_r(r)$ and $B_\theta = B_\theta(r)$ are radial and azimuthal components of $\mathbf{B}_r$, respectively, defined by Eq. (8). On the other hand, the radial component of Eq. (12) is

$$\frac{im}{r}B_z - ikB_\theta = \alpha B_r. \tag{16}$$

However, Eq. (5) requires

$$B_z = \frac{i}{k}\left(\frac{\partial B_r}{\partial r} + \frac{B_r}{r} + \frac{im}{r}B_\theta\right). \tag{17}$$

Thus, the combination of Eqs. (16) and (17) yields B_θ and B_z as function of B_r.

$$B_\theta = \frac{imr\dfrac{\partial B_r}{\partial r} + i(m + \alpha r^2 k)B_r}{m^2 + r^2 k^2}, \tag{18}$$

$$B_z = \frac{ir^2 k\dfrac{\partial B_r}{\partial r} + i(rk - m\alpha r)B_r}{m^2 + r^2 k^2}. \tag{19}$$

Substitution of Eq. (18) into Eq. (15) yields

$$\frac{\partial^2 B_r}{\partial r^2} + \left(1 + \frac{2m^2}{m^2 + r^2 k^2}\right)\frac{1}{r}\frac{\partial B_r}{\partial r}$$

$$+ \left(r^2(\alpha^2 - k^2) - m^2 + \frac{m^2 + kr^2(2m\alpha - k)}{m^2 + r^2 k^2}\right)\frac{1}{r^2}B_r = 0. \tag{20}$$

Thus, B_r is obtained from the uncoupled ordinary differential equation. The total wave number, α, is the eigenvalue of the equation. The relationship between the perturbed electric field and the magnetic field is obtained from Eq. (2).

$$E_r = (\omega/k)B_\theta, \tag{21}$$

$$E_{\theta r} = -(\omega/k)B_r, \tag{22}$$

$$E_z = 0. \tag{23}$$

Two boundary condition cases are considered; insulating boundary and conducting boundary. An insulating boundary requires

$$j_r|_{\text{boundary}} = 0. \tag{24}$$

However, since the current is in the same direction as the perturbed magnetic field by (14), this implies

$$B_r|_{\text{boundary}} = 0. \tag{25}$$

Meanwhile, a conducting boundary requires

$$E_\theta|_{\text{boundary}} = 0. \tag{26}$$

However, Eq. (21) implies

$$B_r|_{\text{boundary}} = 0. \tag{27}$$

Thus, for either the insulating or conducting boundary condition, the radial component of the perturbed magnetic field must vanish at the boundary. Therefore, the boundary conditions are

$$B_r(a) = B_r(b) = 0, \tag{28}$$

$$\frac{\partial B_r(a)}{\partial r} = 1. \tag{29}$$

For an annular helicon source of inner radius a and outer radius b, Eq. (20) is iterated to find eigenvalues, α, such that B_r vanishes at both boundaries. The value of α is strongly

affected by the value of a, which determines the size of the device, and the ratio of b to a, which determines the shape of an annular channel.

A special case arises when a and b are chosen such that the solution of Eq. (20) has zero slope at $r=0$. In this case, the solution can be expressed as a linear combination of Bessel's functions and is identical to the solution for a cylindrically bounded helicon wave, with the first root at $r=a$ and the second root at $r=b$. Thus, the r, θ, and z components of the magnetic field perturbation are

$$B_r = (\alpha + k)J_{m-1}(Tr) + (\alpha - k)J_{m+1}(Tr), \tag{30}$$

$$B_\theta = i[(\alpha + k)J_{m-1}(Tr) - (\alpha - k)J_{m+1}(Tr)], \tag{31}$$

$$B_z = -2iTJ_m(Tr), \tag{32}$$

where T is the perpendicular wave number defined as $T^2 = \alpha^2 - k^2$. Multiplication of Eqs. (30)–(32) by the exponential factor defined by Eq. (8) yields

$$B_r = A[(\alpha + k)J_{m-1}(Tr) + (\alpha - k)J_{m+1}(Tr)]$$
$$\times \cos(m\theta + kz - \omega t), \tag{33}$$

$$B_\theta = -A[(\alpha + k)J_{m-1}(Tr) - (\alpha - k)J_{m+1}(Tr)]$$
$$\times \sin(m\theta + kz - \omega t), \tag{34}$$

$$B_z = 2TAJ_m(Tr)\sin(m\theta + kz - \omega t), \tag{35}$$

and the electric field is expressed as

$$E_r = -A(\omega/k)[(\alpha + k)J_{m-1}(Tr) - (\alpha - k)J_{m+1}(Tr)]$$
$$\times \sin(m\theta + kz - \omega t), \tag{36}$$

$$E_\theta = -A(\omega/k)[(\alpha + k)J_{m-1}(Tr) + (\alpha - k)J_{m+1}(Tr)]$$
$$\times \cos(m\theta + kz - \omega t), \tag{37}$$

$$E_z = 0. \tag{38}$$

Thus, the solution is expressed explicitly for this special case, in which the solution is identical to that of cylindrical case. In general, the radial component of the perturbed magnetic field is obtained with Eq. (20) and the boundary conditions given by Eqs. (28) and (29). This result is substituted into Eqs. (18) and (19) to obtain the azimuthal and axial components of the magnetic field. The perturbed electric field shape is obtained from Eq. (21)–(23). For the ratio of b to a applicable to HETs, the special case closed-form solution described by Eqs. (33)–(38) yields the qualitative behavior of the plasma source.

III. MODE SHAPE ANALYSIS

As Eqs. (18)–(20) show, there are infinitely many solutions that satisfy the governing Eqs. (2)–(4). The mode number, m, governs the field patterns. There have been many successful generations of $m=-1,0,1$ mode helicons in the laboratory environment.[1,4] These experiments show that antenna coupling is easiest to accomplish in the $m=1$ mode. Further, the highest plasma density has been achieved in $m=1$ mode, for a given magnetic field strength and input
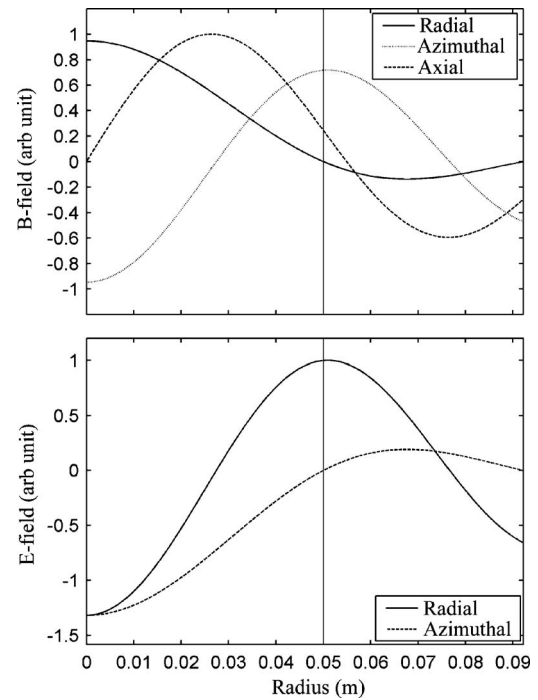

FIG. 2. Magnetic and electric field variation with radius.

power.[4] Therefore, the $m=1$ mode helicon wave is studied in detail in this section. Figure 2 shows electric and magnetic field profiles for the special case mentioned earlier. The region between 0 and 0.05 m corresponds to the solution for a cylindrically bounded helicon wave, with a source radius of 0.05 m. The region between 0.05 and 0.092 m corresponds to the solution for an annularly bounded helicon wave, with an inner radius of 0.05 m and a outer radius of 0.092 m. B_r vanishes at both the inner boundary ($r=0.05$ m) and the outer boundary ($r=0.092$ m), which satisfies the boundary conditions posed by Eq. (28). The wave patterns for the special case depicted in Fig. 2 hold in general for the range of outer to inner radius of interest.

Figure 3 shows a typical field pattern of an annularly bounded helicon wave. The electric field lines are perpendicular at the both boundaries, as the radial component of the magnetic field must vanish at these points as shown by Eq. (28) and the electric field is perpendicular to the magnetic field. A stationary observer sees the pattern rotate in the right-handed sense with respect to the applied magnetic field. The electric field in the inner region is much stronger than the outer region. Thus, an antenna can be designed to couple to the strong electric field region in the upper and the lower inner region of the plasma. This is similar to the antenna coupling in the center region for a cylindrically bounded wave.[3]

IV. ENERGY DEPOSITION

The rf energy deposition per unit volume is calculated as the dot product of the current density and the electric field. However, only the axial component of the current and the electric field result in energy loss, as the transverse compo-
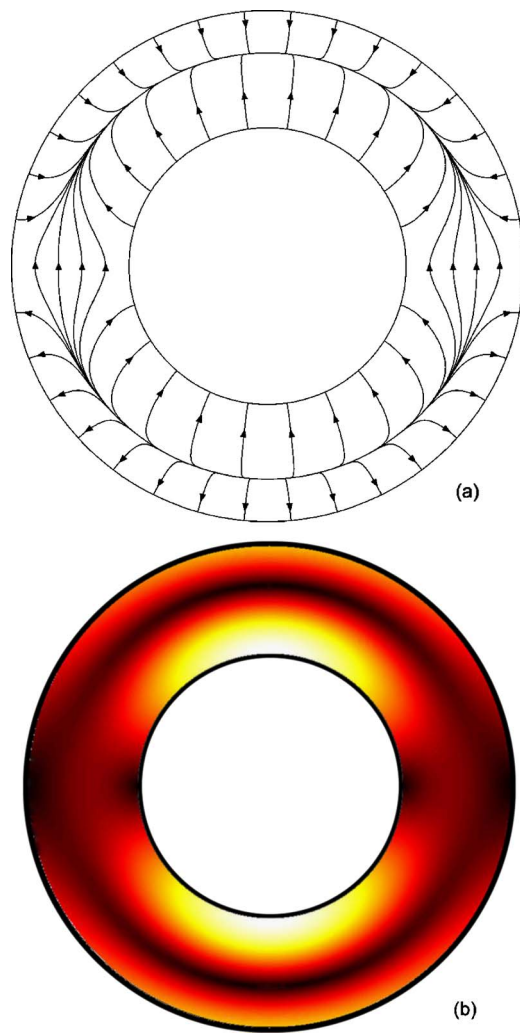
(a)

(b)

FIG. 3. (Color online). The electric field pattern for the $m=1$ mode for $k/\alpha=0.1$. The line spacing is not indicative of the electric field strength (a). Lighter color represents the region of strong electric field, and darker color represents the region of weak electric field (b).

FIG. 4. Radial energy deposition profile at two different values of k/α. The inner radius is 0.06 m and the outer radius is 0.09 m.

nents of the electric field and the current are perpendicular to each other by Eqs. (14), (21), and (22). Thus, the energy loss rate per unit volume can be computed as

$$-\frac{dW}{dt} = \mathbf{j} \cdot \mathbf{E} = j_z E_z. \tag{39}$$

Although Eq. (23) indicates that the axial component of the electric field is equal to zero, the equation was derived assuming zero resistivity. In presence of damping, the axial electric field becomes nonzero, as it must drive the axial current. In helicon sources, rf energy is absorbed through both collisional and collisionless damping mechanisms. In particular, Chen has pointed out the very efficient rf energy absorption in helicon devices may be due to Landau damping.[3] Relative magnitude of the energy absorption rate per unit volume can be approximated as ηj_z^2 without detailed consideration of the damping mechanism, where η is resistivity and j_z is approximately equal to that of the undamped solution with weak damping. By Eq. (14), the axial current is
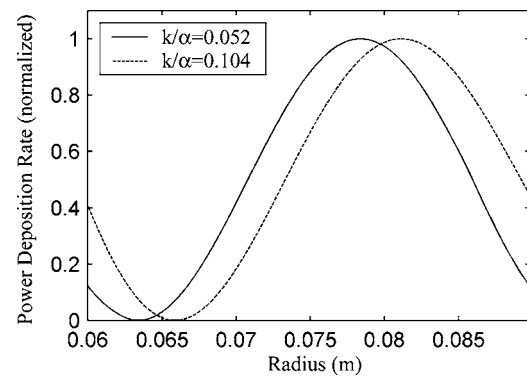
$$j_z = (\alpha/\mu_0)B_z, \tag{40}$$

and the energy absorption rate per unit volume is

$$\dot{W} = \eta(\alpha/\mu_0)^2 B_z^2. \tag{41}$$

If the dominant collision mechanism is either the electron-neutral collision or Landau damping, then the resistivity is inversely proportional to the density.[3] By Eq. (11), the density, n_0, is proportional to the total wave number, α, for a given phase velocity and applied magnetic field strength. Thus, η is inversely proportional to α. The energy absorption rate is proportional to

$$\dot{W} \propto |\alpha| B_z^2. \tag{42}$$

Therefore, the energy deposition rate is proportional to B_z^2.

Figure 4 shows the energy deposition profiles for two different values of k/α. The energy deposition curve shifts outward as k/α increases, which corresponds to an increase in the excitation frequency or a decrease in applied magnetic field strength for a fixed annular channel geometry by Eq. (11). The region of high energy absorption rate is suspected to produce the greatest number of high-energy electrons through Landau damping. Thus, for maximum confinement of the high-energy electrons it is desirable to keep the energy deposition peak near the center of the channel. Furthermore, these high-energy electrons create high-energy ions through electron-neutral collisions. As erosion of the discharge channel wall by high-energy ions limits HET lifetime, confinement of the high-energy ions to the center of the channel may increase their lifetime. Thus, it is desirable to design a source with a low k/α value to keep the region of the peak energy deposition near the center of the channel. For a cylindrical source, experiments have shown that energy deposition profile is not as narrow as the profile predicted by the theory.[3] The broader energy deposition profile can be attributed to nonuniform density profile created by diffusion, which is not considered in the calculation. Diffusion is expected to induce a similar effect to an annularly bounded helicon source.
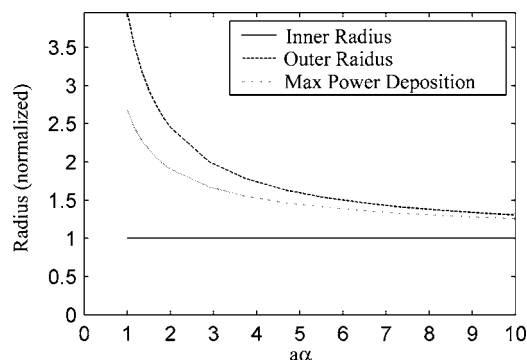
FIG. 5. Variation of outer radius and maximum energy deposition radius with $a\alpha$.

FIG. 6. Variation of outer radius, minimum energy deposition radius, and maximum energy deposition radius with k/α.

V. PARAMETRIC STUDY

To characterize the field pattern of annularly bounded helicon waves, several variables are introduced. Let a and b be the inner and the outer radius, and r_{max} and r_{min} be the radius of maximum and minimum energy absorption, respectively. Equation (42) shows that the energy deposition rate varies as B_z^2. Therefore, the maximum energy deposition occurs where the axial magnetic field is maximum and energy deposition reaches zero at the point where the axial magnetic field reverses direction.

Figure 5 shows the variation of the outer radius and the maximum power deposition radius with $a\alpha$ for a fixed inner radius. Although this calculation is done for a case with a nondimensional parameter $k/\alpha=0.1$, a similar variation is observed for any value of k/α. As Fig. 5 shows, the value of $a\alpha$ strongly affects the ratio of outer to inner radius. On the other hand, the location of maximum energy absorption radius relative to the inner and outer radius only changes slightly with the value of $a\alpha$.

Figure 6 shows a typical variation of outer radius, maximum energy absorption radius, and minimum energy deposition radius as functions of k/α. As the graph shows, the outer radius decreases slightly with k/α at low k/α value, but it increases with k/α at high k/α. The variation of the outer radius with k/α is relatively small compare to the ef-
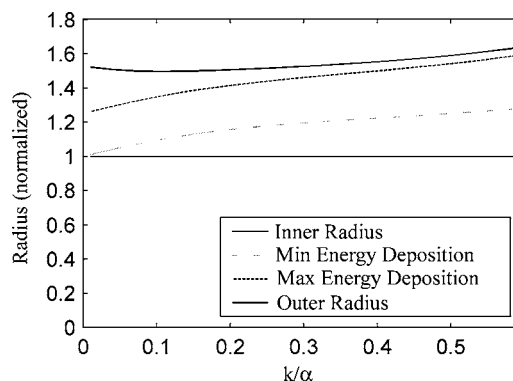
fect the value of $a\alpha$ have on the outer radius, which is depicted in Fig. 4. On the other hand, k/α strongly affects the location of the maximum and the minimum energy deposition. Increase in the value of k/α pushes the energy deposition profile outward.

VI. CONCLUSION

The analysis shows that it is possible to solve the electric and magnetic field equation for the boundary conditions of a coaxial helicon plasma source. Moreover, the electric field pattern in the $m=1$ mode provides a feasible location for a rf antenna to couple to the plasma. The variation of the energy deposition profile with respect to k/α shows the need to drive the antenna at lower frequency to position the peak energy deposition near the center of the channel for a given phase velocity. The variation of the outer radius and the peak energy deposition radius with respect to the value of $a\alpha$ and k/α shows that $a\alpha$ primarily affects the outer radius while k/α affects the location of the peak energy deposition.

[1] R. W. Boswell, Plasma Phys. Controlled Fusion **26**, 1147 (1984).
[2] R. R. Hofer and R. S. Jankovsky, 37th Joint Propulsion Conference and Exhibit, Salt Lake City, UT, July 8–11, 2001, Paper No. AIAA-2001-3322.
[3] F. F. Chen, Plasma Phys. Controlled Fusion **33**, 339 (1991).
[4] I. D. Sudit and F. F. Chen, Plasma Sources Sci. Technol. **5**, 43 (1996).